Numerical methods for calculating the response of a deterministic and stochastically excited Duffing oscillator

David H Hawes and Robin S Langley
Department of Engineering, University of Cambridge, UK
Email: dhh29@cam.ac.uk

Abstract

When compared to independent harmonic or stochastic excitation, there exist relatively few methods to model the response of nonlinear systems to a combination of deterministic and stochastic vibration despite the likelihood of harmonic oscillations containing noise in realistic applications. This paper uses the Duffing oscillator to illustrate how the joint probability density function (JPDF) of the displacement and velocity responds to this form of excitation. Monte-Carlo simulations were performed to generate the JPDF which was observed to spread around the attractor that would be seen if only deterministic excitation was present. This paper assesses the ability of a useful class of methods, global weighted residual methods, to produce the geometrically complex JPDF responses produced from harmonic and white noise excitation. A technique using a JPDF in the form of a Gram-Charlier type C series was found to produce accurate results, although the method fails due to ill-conditioning as the shape of the JPDF required by the dynamics becomes too complex.

Keywords: Nonlinear, Stochastic, Deterministic, Vibration, Duffing

1 Introduction

When analysing real engineering applications mathematically, many vibration problems are approximated to systems that are either harmonically or randomly excited. However, in many cases broadband noise with a series of harmonics is exhibited or deliberately generated such as the response of a helicopter,[1] vibration of turbine blades under turbulent flow[2] and stochastic resonance.[3] More recently, this form of excitation is of interest in the field of energy harvesting, where devices are tuned to operate within a narrow frequency band and their robustness to disturbances from noise must be assessed.[4] Although still an idealisation, excitation modelled as a sinusoid superimposed onto broadband noise can more closely resemble the realistic case and should therefore more accurately model the system dynamics than approximating the excitation as simply harmonic or broadband noise.

A number of techniques have been used to model nonlinear responses to this form of excitation and range from approximate analytical to numerical methods. The former generally involve a combination of deterministic and stochastic nonlinear techniques to generate and solve coupled harmonic and noise equations. The methods proposed in the literature include equivalent linearisation of the coupled equations from mean and random terms,[5,6] the method of multiple scales used with an appropriate closure technique,[7,8] deterministic and random perturbation analysis[9] and stochastic averaging with equivalent linearisation,[10,11] with solving the resulting Fokker-Planck equation[12] and with harmonic balance.[13] These methods have shown reasonable accuracy and generate rapid solutions. However, the results are limited by the approximations made in order to generate solvable equations. If further accuracy is desired, numerical approaches are required.

In the literature the numerical techniques for harmonic and broadband excitation can be seen as an extension of methods that solve the non-stationary Fokker-Planck equation. The finite difference,[14,15] finite element,[15–17] path integration[18–21] and cell[14,22] method are all applicable to non-stationary excitation and have been used to investigate combined harmonic and broadband excitation.

Of particular interest in this paper are global weighted residual solutions which have been applied to random vibration problems. These involve proposing the form of the probability density function (PDF) with unknown coefficients and substituting it into

the Fokker-Planck equation. Since the PDF will generally not satisfy this equation, a residual error will occur which can be minimised by being multiplied by a suitable weighting function and integrated over the entire state-space. A number of weighted integrals can be taken to generate a simple set of equations that are solved to find the coefficients that govern the shape of the PDF. In these solutions, the results depend on selection of a suitable proposed PDF that can reasonably approximate the true PDF and selection of suitable weighting functions that project the solution onto the relevant regions of state space.

A proposed PDF in the form of a sum of Gaussian distributions with state variables of varying exponent as weighting functions has been investigated,[23] but found to have limited accuracy for responses far from Gaussian. An exponential function containing polynomials of the state variables has been used as the PDF with state variables of varying exponent multiplied by a Gaussian distribution used as weighting functions.[24,25] The sensitivity to the standard deviation used in the Gaussian weighting function is shown[25] to be important and a method for selecting sensible weight functions has been devised and shown to work well.

A Gram-Charlier type A series has been used as the proposed PDF and Hermite polynomials are used as weighting functions such that their orthogonality can be exploited to enable rapid solution.[26,27] The Gram-Charlier type A series is limited in that it permits negative probabilities and only near to Gaussian responses so the Gram-Charlier type C series which accounts for polynomial qualities of the logarithm of the PDF has been used and produced strong results.[28] A similar method has been applied successfully to harmonic and noise excitation of a first order system.[29]

Another improvement on the Gram-Charlier type A method[26,27] is to use a more accurate distribution multiplying the polynomial series than the Gaussian of a Gram-Charlier type A series. This could come from equivalent linearisation, a known analytical solution of a similar Fokker Planck equation[30] or stochastic averaging to find the PDF of the peak responses.[31–33] A set of orthogonal polynomials can then be created and solved for this distribution. These methods have shown good accuracy and work well for higher order systems.

A method that has produced good results in the physics literature is the method of matrix continued fractions.[34,35] It is similar to the weighted residual methods discussed above, but instead of solving coupled algebraic or differential equations for the

stationary or non-stationary cases respectively, it solves for the PDF coefficients by noting that the equations from the weighted residuals can be formed into a tri-diagonal recurrence relation and therefore solved using matrix continued fractions.

This paper aims to investigate how global weighted residual solutions can be extended to model nonlinear oscillators under combined harmonic and white noise excitation. In what follows, the response of the Duffing oscillator to this form of excitation is presented using Monte-Carlo simulations to generate the JPDF of the response. Two weighted residual methods are then described and their accuracy and limitations are investigated by comparing them to results from Monte-Carlo and path integration methods.

2 Monte-Carlo simulations

This section aims to illustrate the dynamics of an oscillator under combined deterministic and random excitation by investigating the Duffing oscillator's response to sinusoidal and white noise excitation using Monte-Carlo simulations. Similar results have previously been shown using a variety of methods[10,14,19–21,36,37] and agree with those presented here.

The equation describing a Duffing oscillator under harmonic and white noise forcing is

$$\ddot{x} + c\dot{x} + kx + \epsilon x^3 = F\cos(\omega t) + W(t) \tag{1}$$

where $W(t)$ is a white noise process such that its autocorrelation function

$$E[W(t)W(t-\tau)] = \pi S_0 \delta(\tau) \tag{2}$$

where $E[X]$ represents the ensemble average of X, $\delta(\tau)$ is the Dirac delta function and S_0 is the single-sided spectral density.

The Monte-Carlo method is a simple but computationally expensive technique for generating the JPDF of the response. The oscillator of equation (1) is excited by a large number of realisations of the random forcing. The ensemble of responses are found using the ode45 time integration function in MATLAB and then the likelihood of the response displaying a given displacement and velocity at a given time can be found from the proportion of realisations that display this displacement and velocity at each time step.

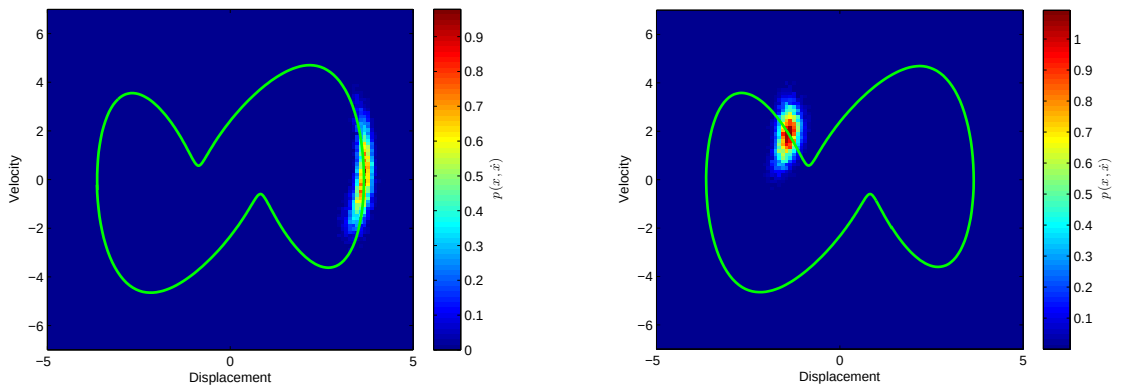

(a) (b)

Figure 1: JPDFs from Monte-Carlo simulations of response to combined harmonic and random excitation at a) $t = 28.4$ and b) $t = 32.4$ when $c = 0.7$, $k = 0.5$, $\epsilon = 0.5$, $F = 10$, $\omega = 1$ and $S_0 = 0.05$. The response over one cycle for purely harmonic forcing is superimposed.

Figure 1 shows the Monte-Carlo JPDF in the phase plane for the Duffing oscillator of equation (1) at two times when $c = 0.7$, $k = 0.5$, $\epsilon = 0.5$, $F = 10$, $\omega = 1$ and $S_0 = 0.05$ and an ensemble of 10000 realisations. The Monte-Carlo simulations presented in this paper have initial conditions $x(0) = \dot{x}(0) = 0$. However, the figures display the responses when the system is at steady-state at times that illustrate the characteristic dynamics. It can be seen that the response follows the deterministic trajectory superimposed onto the figure and the noise perturbs the response about the deterministic case.

The ensemble average of the response of the noisily forced oscillator, found from the steady-state JPDF over one cycle of the harmonic component of the forcing, is compared with the mean trajectory when only harmonic forcing is applied in Figure 2. The mean response is affected by the presence of the white noise, but still displays approximately the same path.

When subjected to harmonic excitation, nonlinear oscillators can produce complex responses such as exhibiting more than one steady-state response depending on initial conditions and chaotic solutions. It is interesting to investigate the response of such systems when noise is added to the excitation. A simple example of the former case is when a Duffing oscillator is excited harmonically such that it exhibits either a high

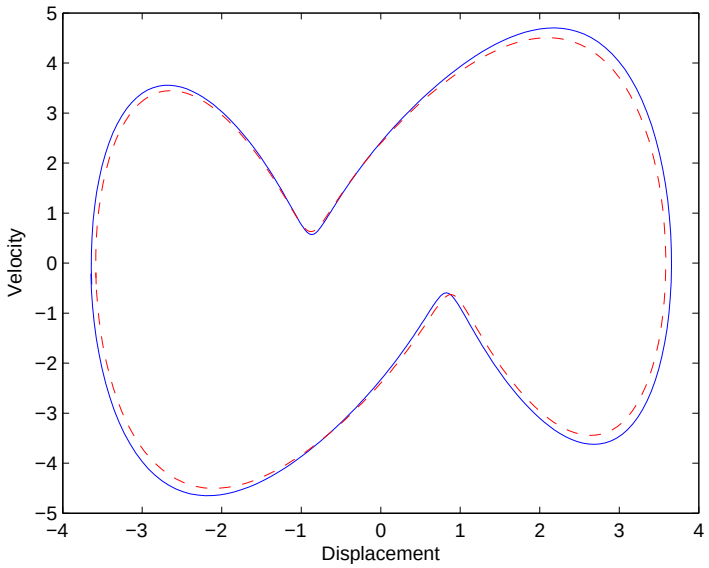

Figure 2: Mean response of harmonically excited oscillator with (dashed) and without (solid) noise.

or low magnitude orbit. The JPDF of this case is displayed in Figure 3 at two times when $c = 0.5$, $k = 0.5$, $\epsilon = 0.5$, $F = 10$, $\omega = 3.05$ and $S_0 = 0.8$ and 20000 realisations. Similar to the simple case of Figure 1, the response spreads around one or other of the deterministic orbits and the noise can make the response jump from oscillations about one orbit to oscillations about the other.

When a nonlinear oscillator is harmonically excited a chaotic response can be observed that is both non-periodic and sensitive to its initial conditions. Chaotic systems contain an underlying fractal structure that can be uncovered by sampling the response at the frequency of the harmonic forcing in the phase plane to find a 'Strange Attractor'. In the periodic solutions above with noise and harmonic excitation, the JPDF spreads out around the periodic trajectory that would be observed if only harmonic excitation were applied. However, in the deterministic chaotic case there is no periodic trajectory for the response to spread around and the trajectory is extremely sensitive to small perturbations from noise. As can be seen from Monte-Carlo simulations of a chaotic system in Figure 4, when noise is added to the harmonic excitation the JPDF remains close to fractal, similar to a strange attractor, but it has diffused slightly due

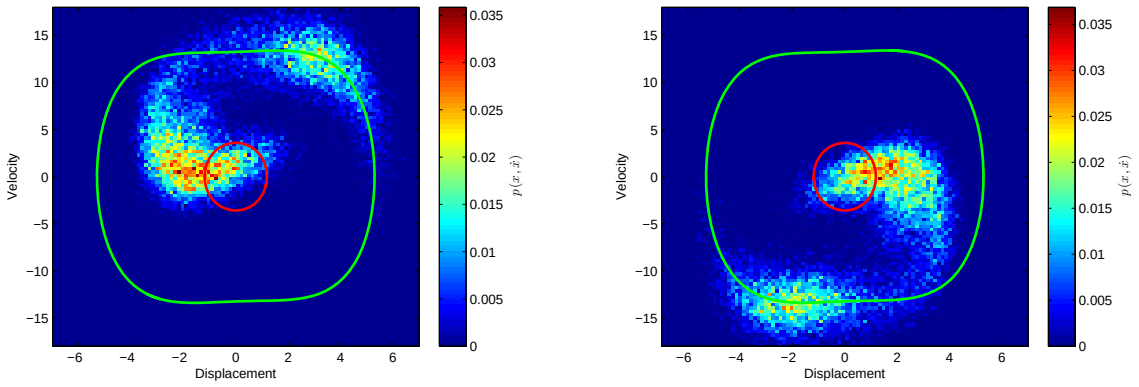

(a) (b)

Figure 3: JPDF from Monte-Carlo simulations of Duffing oscillator excited in a configuration where, under harmonic excitation, two responses (solid lines) exist. $c = 0.5$, $k = 0.5$, $\epsilon = 0.5$, $F = 10$, $\omega = 3.05$ and $S_0 = 0.8$, a) $t = 34$ and b) $t = 37$.

to the noise. With noise added to the harmonic excitation, the chaotic case is therefore similar to the periodic cases above in that the noise spreads the JPDF around the deterministic attractor although in the chaotic case, the individual realisations can differ dramatically.

Diffuse chaotic attractors from noisy and harmonic excitation have been simulated using the path integration method and the possibility of using a no-noise limiting case of stochastic methods to model deterministic chaos has also been discussed.[37] A time-invariant PDF of a noisy chaotic response averaged over one forcing period has been calculated using the matrix continued fractions method and assuming the PDF's response is periodic.[36] The necessary periodicity of the response has been discussed and the effect of increasing noise is shown to generate a more diffuse attractor.[36] The periodicity is illustrated here in Figure 5 by observing the mean square velocity of the Monte-Carlo results over time. The periodic nature at steady-state suggests that the JPDF's moments are periodic so it may be possible to obtain useful information about the chaotic response despite not being able to mathematically describe the complex shape of the JPDF.

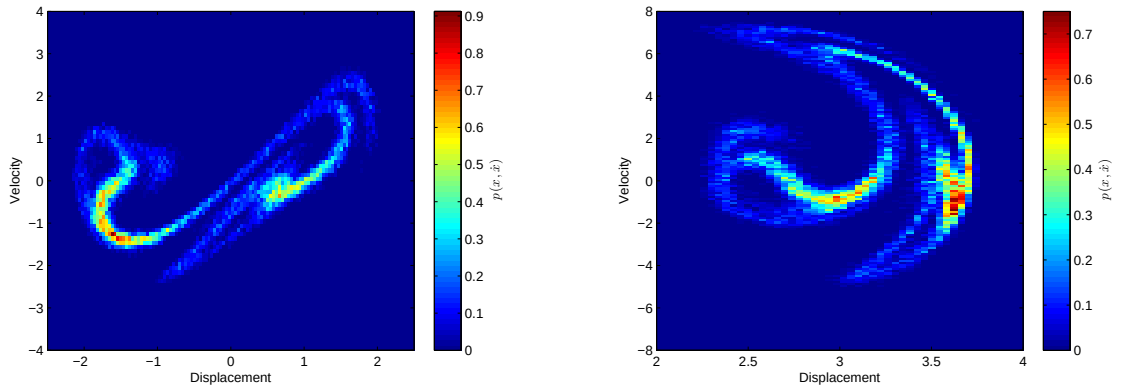

(a) (b)

Figure 4: JPDFs at time a) $t = 141.1$ and b) $t = 142.8$ from Monte-Carlo simulations of a bi-stable Duffing oscillator with a noisy chaotic response. $c = 0.1$, $k = -0.5$, $\epsilon = 1$, $F = 10$, $\omega = 1$ and $S_0 = 1 \times 10^{-3}$ and 20000 realisations.

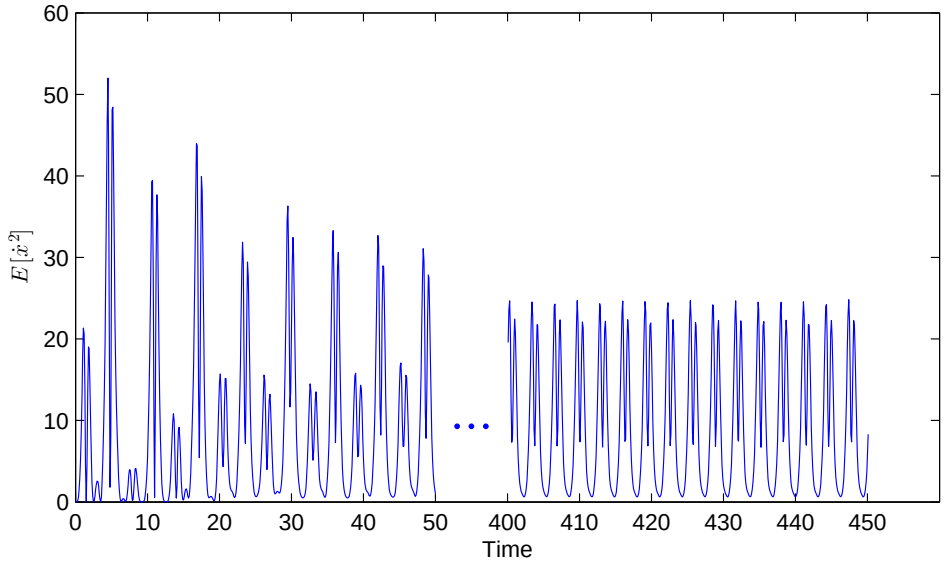

Figure 5: Time history of mean squared velocity of chaotic response.

3 Global weighted residual methods

In the light of the complexity of a noisy chaotic attractor and the computational expense of Monte-Carlo and path integration methods, it is interesting to investigate how the global minimisation properties of the weighted residual methods attempt to generate complex instantaneous attractor geometries. In this section two weighted residual methods are taken from the literature and extended to model the response to harmonic and white noise excitation then compared to Monte-Carlo and path integration results.

3.1 Theory

In a weighted residual method, the form of the proposed PDF is important as it dictates the range of possible shapes the PDF can display. Two different proposed PDFs, p_A and p_C, are compared in this section; the Gram-Charlier type A series, equation (3), and Gram-Charlier type C series, equation (4), and relevant solution methods[27,28] are used. These two methods were chosen because they can be solved similarly, are simple and elegant due to the use of Hermite orthogonality and should be representative of the majority of weighted residual methods.

$$p_A(z,\dot{z},t) = C\exp\left(-\frac{z^2}{2}-\frac{\dot{z}^2}{2}\right)\sum_{m=0}^{\infty}\sum_{n=0}^{\infty}a_{mn}(t)H_m\left(z\right)H_n\left(\dot{z}\right) \tag{3}$$

$$p_C(z,\dot{z},t) = C\exp\left[\sum_{m=0}^{\infty}\sum_{n=0}^{\infty}a_{mn}(t)H_m\left(z\right)H_n\left(\dot{z}\right)\right] \tag{4}$$

where C is a normalisation constant such that $\int_{-\infty}^{\infty}\int_{-\infty}^{\infty}p\,dxd\dot{x}=1$ and a_{mn} are time varying coefficients to be found. $H_n(z)$ is a nth order Hermite polynomial defined as

$$H_n(z) = (-1)^n e^{\frac{z^2}{2}}\frac{\mathrm{d}^n}{\mathrm{d}z^n}e^{-\frac{z^2}{2}} \tag{5}$$

where

$$z(t) = \frac{x-x_m(t)}{\sigma_x(t)} \tag{6}$$

$$\dot{z}(t) = \frac{\dot{x}-\dot{x}_m(t)}{\sigma_{\dot{x}}(t)} \tag{7}$$

and $x_m(t)$, $\dot{x}_m(t)$ and $\sigma_x(t)$, $\sigma_{\dot{x}}(t)$ are estimates of the mean and standard deviation of the displacement and velocity respectively found from an equivalent linearisation

method for non-stationary excitation.[5] The transformation from x to z is used to ensure that the JPDF is defined around the deterministic response as suggested from the results of the Monte-Carlo simulations section and is scaled to an appropriate magnitude according to the noise present. This transformation is not appropriate for the chaotic case since it does not spread around the deterministic trajectory.

A proposed PDF is substituted into the relevant Fokker-Planck equation

$$\mathscr{L}(p) = \frac{\partial p}{\partial t} + \dot{x}\frac{\partial p}{\partial x} - \frac{\partial p g(\dot{x}, x, t)}{\partial \dot{x}} - \pi S_0 \frac{\partial^2 p}{\partial \dot{x}^2} = 0 \tag{8}$$

where $g(x, \dot{x}, t) = c\dot{x} + kx + \epsilon x^3 - F\cos(\omega t)$. The Duffing nonlinearity is taken here as an example, but any integer power nonlinearity could be used.

The substitution of either equation (3) or (4) into equation (8) will not be equal to zero in the nonlinear case with a finite Gram-Charlier series thus a residual error, Δ, remains such that $\Delta_A = \mathscr{L}(p_A)$ and $\Delta_C = \mathscr{L}(p_C)$. Using the well-known Galerkin method, this residual can be multiplied by appropriate weighting functions and minimised by integrating over state space. The weighted integrals for the Gram-Charlier type A and C series are

$$\int_{-\infty}^{\infty}\int_{-\infty}^{\infty} H_r(z)H_s(\dot{z})\Delta_A \mathrm{d}\dot{z}\mathrm{d}z = 0 \tag{9}$$

$$\int_{-\infty}^{\infty}\int_{-\infty}^{\infty} H_r(z)H_s(\dot{z})e^{-\frac{z^2}{2}-\frac{\dot{z}^2}{2}}\frac{1}{p_C}\Delta_C \mathrm{d}\dot{z}\mathrm{d}z = 0 \tag{10}$$

where the orthogonality properties of Hermite polynomials, equations (11) and (12), have been exploited to greatly reduce the number of terms in the resulting equations.

$$\int_{-\infty}^{\infty} H_r(z)H_n(z)e^{-\frac{z^2}{2}}\mathrm{d}z = \sqrt{2\pi}n!\delta_{rn} \tag{11}$$

$$\int_{-\infty}^{\infty} H_r(z)H_m(z)H_n(z)e^{-\frac{z^2}{2}}\mathrm{d}z = \begin{cases} \frac{\sqrt{2\pi}r!m!n!}{(s-r)!(s-m)!(s-n)!} & r+m+n \text{ even} \\ 0 & r+m+n \text{ odd} \end{cases} \tag{12}$$

where $2s = r + m + n$.

It is clear that for computation of this method, the infinite Gram-Charlier series must be truncated in some way. A truncation method known to produce good results[28] is adopted and involves removing terms above a chosen order, N, such that $m + n \leq N$. In the weighted integrals of equations (9) and (10), r and s therefore vary from

$0 \to N - s$ and $0 \to N - r$ respectively to produce a number of coupled differential equations of the form

$$\frac{\mathrm{d}a_{rs}}{\mathrm{d}t} = f_{rs}(a_{00}, a_{10}, a_{01}, a_{11}...) \tag{13}$$

that can be solved using a numerical ODE solver such as ode45 in MATLAB to yield the required a_{mn} coefficients.

3.2 Results

The results found from the weighted residual methods (abbreviated to WR-A and WR-C for type A and C respectively) will now be compared in terms of accuracy and speed to results from Monte-Carlo simulations (MC) and the path integration method[19] (PI) and described in the appendix. Despite the noise, the MC simulations will be taken as the benchmark, since the method most realistically models the dynamics provided a large enough ensemble is taken.

A qualitative comparison of the results is shown for a strongly nonlinear, highly damped oscillator in Figure 6 where the JPDFs at two times are shown using each of the methods and Figure 7 provides a more quantitative comparison by comparing only the displacement PDFs. The WR-A method shows poor similarity to the MC simulations and regions of negative probability in Figure 7(a) whereas it provides a reasonable approximation in Figure 7(b). The PI method does not appear to produce the complexity of the MC JPDF and its mean value is incorrect in Figure 7(b).

The WR-C results provide a good approximation of the Monte-Carlo simulations, although the tail probability in Figure 7(b) is less accurate. This is due to the form of the Gram-Charlier type C series meaning that when the JPDF is constructed, it can produce regions of exponentially growing probability away from the mean response. To ensure these high probabilities do not affect the JPDF in the region of interest, only the probabilities in the vicinity of the mean are taken. This also increases the speed of the construction of the JPDF since calculations are only performed in regions of significant probability. The effect of this truncation is observed in Figure 7(b) where the displacement PDF does not drop smoothly to zero, but has been truncated abruptly. It appears the method is providing a good approximation to the true response in the vicinity of the mean motion, but worse results elsewhere. This is discussed further in the limitations section below.

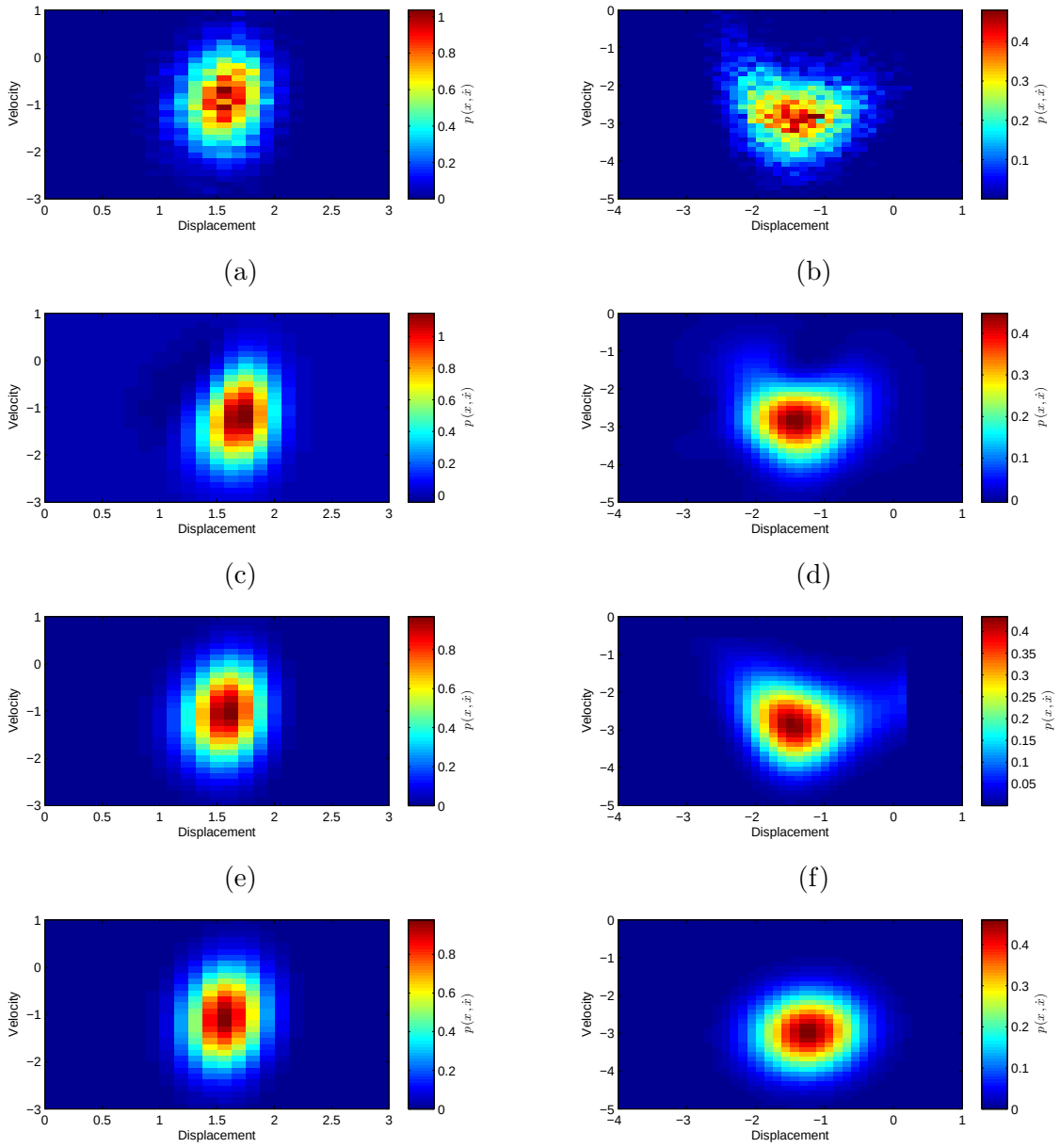

Figure 6: JPDFs from MC a) and b), WR-A c) and d), WR-C e) and f) and PI g) and h) at times $t = 17.3$ a), c), e) and g) and $t = 18.8$ b), d), f) and h). $c = 3.0$, $k = -0.5$, $\epsilon = 1$, $F = 10$, $\omega = 1$ and $S_0 = 0.5$.

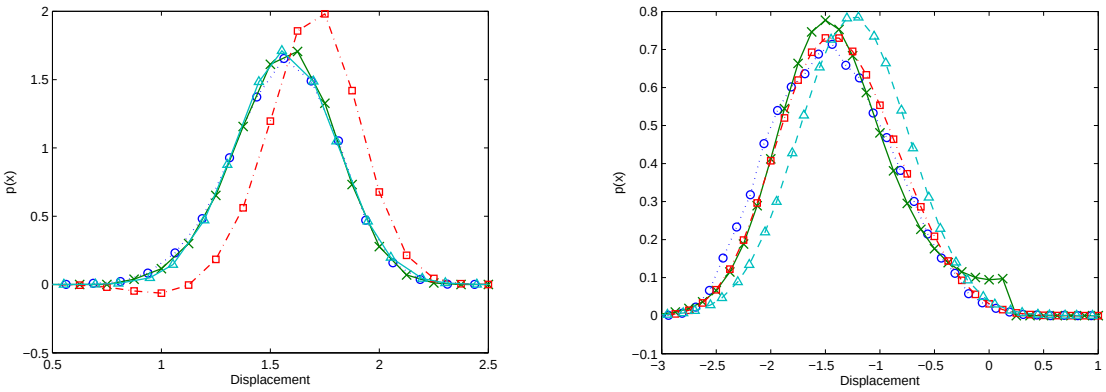

(a) (b)

Figure 7: Probability density functions of displacement from MC (dotted line with circles), WR-A (dash-dot line with squares), WR-C (solid line with crosses) and PI (dashed line with triangles) methods at times a) $t = 17.3$ and b) $t = 18.8$.

In order to compare the statistical moments retrieved from each method, the variation of the mean square velocity has been plotted against time in Figure 8. The equivalent linearisation and WR-C method show almost identical results and both closely resemble the MC solution. Negative mean square velocity values are displayed for the WR-A solution suggesting there are times when the JPDF is largely negative and therefore extremely inaccurate. The JPDF using the PI method is only solved for every quarter cycle, and generates results slightly worse than equivalent linearisation and WR-C.

For the solutions above, an ensemble of 10000 realisations was used and the weighted residual solutions were truncated at $N = 5$ and $N = 3$ for the type A and C respectively. For the type A solution, the value was selected since a smaller value shows little divergence from the Gaussian JPDFs of equivalent linearisation results whereas a larger value produces highly inaccurate and negative JPDFs. For the type C solution, the value was chosen high enough to allow for a complex JPDF shape, but low enough to avoid ill-conditioning as discussed in the limitations section below.

For the case shown in Figures 6 to 8 the times taken to compute the response are displayed in Table 1, where the equations were solved from $t = 0$ to $t = 20$ with a time step, $\mathrm{d}t$, of $\mathrm{d}t = 0.01$ for the MC and weighted residual methods, and a time step of a quarter of the period of the harmonic excitation frequency, $\mathrm{d}t = 1.6$, for the PI

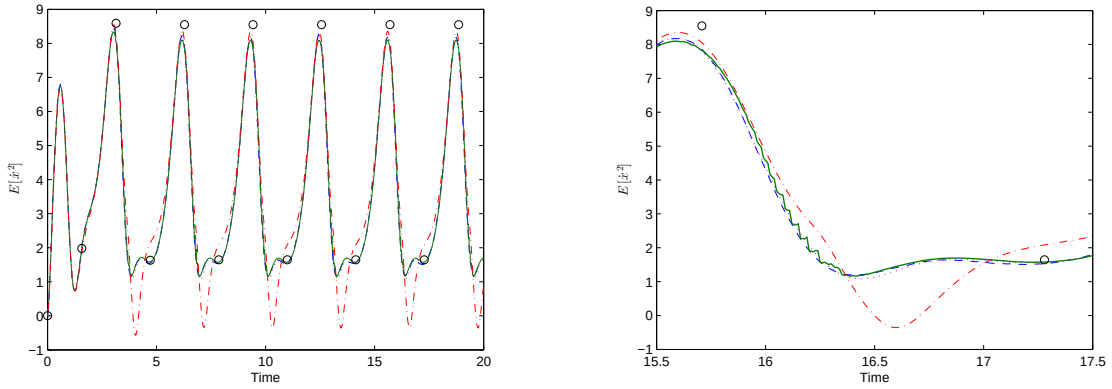

(a) (b)

Figure 8: Mean square velocity against time from MC (dashed), WR-A (dash dot), WR-C (solid), PI (circles) and equivalent linearisation (dotted). b) Shows an enlarged view of the time history in a).

method. An 80×80 grid in the phase-plane has been used for each method.

Table 1: Computation time for solution methods.

Method	**Computation Time (s)**
Monte-Carlo	1.4×10^4
Weighted Residual type C	4.5
Weighted Residual type A	6.8
Path Integration	64
Equivalent linearisation	0.78

It is clear that the MC method is the slowest, although it strongly depends on the accuracy of the response desired and therefore the ensemble size used. The weighted residual methods solve rapidly and the accuracy of the JPDF from the type C solutions suggests it is an appropriate method to use for investigating this form of excitation if a fast method is required. However, depending on the desired information, the equivalent linearisation method may be sufficient.

The path integration method is known to be robust and able to produce complex JPDF shapes. In this case however, the results have shown worse accuracy than the

WR-C solutions and taken longer to perform. Additionally, the solution is only found at each quarter cycle and using shorter time steps would require significantly more computational effort. It should be noted that only a simple PI method[21] has been investigated and modifications may improve the method significantly.

3.3 Limitations of the weighted residual type C method

The weighted residual type C method produces good results for the parameters chosen above, but has obvious limitations due to the possible shapes made available by the truncated Gram-Charlier type C series (e.g. the JPDF will never be fractal like the chaotic case). Additionally, it has been observed that when the parameters require a JPDF too complex for the shapes allowed by equation (4), the ODEs of equation (13) will become unstable and fail to solve.

These coupled equations have been investigated to assess the cause of the instability. The dependence of the right hand side of each individual equation on each a_{mn} coefficient is found by differentiating every equation by every coefficient. A matrix, K_{ij}, is therefore formed where $K_{ij} = \partial f_i / \partial a_j$ if f_{rs} and a_{mn} are written as vectors f_i and a_j. The condition number of this matrix gives an indication of the conditioning of the equations and has been plotted against time in Figure 9 for a high damping case that provides a stable solution and a lower damping case that goes unstable at $t = 5.2$. The sharp peak in condition number at this point, along with the preceding peaks show that the equations are ill-conditioned therefore numerical errors grow with time leading to instability.

Observing the JPDF at the point of instability illuminates more physically what occurs in the unstable equations. The JPDF is projected by the Gaussian distribution in the weighting function of equation (10) into a region around the mean response. The weighted residual solutions will therefore model the response well in this region, but at the expense of an accurate JPDF further from the mean. This often results in areas of large probability far from the mean that are removed by truncating the JPDF as described in the results section. When the dynamics requires a complex JPDF shape, in order to approximate it near the mean, the global minimisation of the weighted residuals allow the response just away from the mean to be less accurate. The equations have been seen to become unstable when the true JPDF becomes a

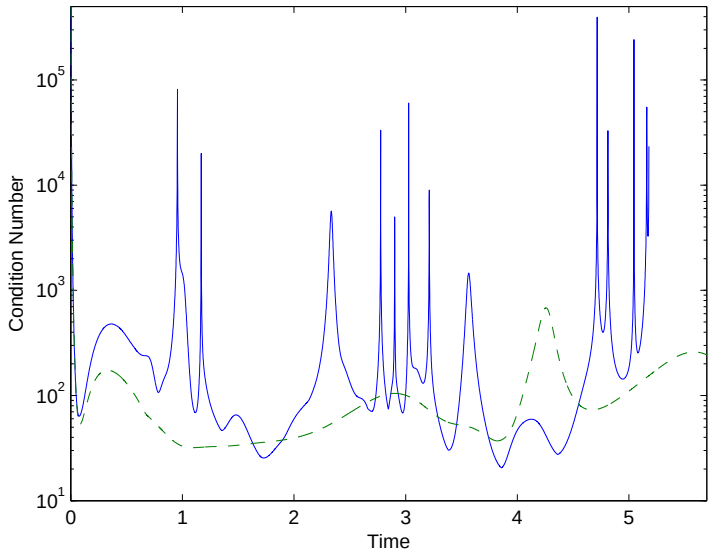

Figure 9: Condition number against time $c = 1$ (solid) and $c = 4$ (dashed) and $k = -0.5$, $\epsilon = 1$, $F = 10$, $\omega = 1$ and $S_0 = 0.5$.

complex shape and cannot be satisfactorily modelled by the truncated Gram-Charlier type C series. At this time, anomalous external regions of high probability are seen to move towards and merge with the JPDF around the mean.

A number of parameters affect the stability of the solution. In particular, the order of the truncated Gram-Charlier series affects the number of coupled equations and the number of terms in each equation. It is therefore found that truncation at a lower value generates stable solutions that are less accurate whereas truncation at higher values produce ill-conditioned equations that show greater accuracy due to a greater range of JPDF shapes allowable. This effect is shown in Figure 10 where an error, e, from the difference between the MC and weighted residual results' mean square velocity is taken such that

$$e = \frac{1}{T\sigma_{\dot{x}}^4} \int_0^T (\mathrm{E}[\dot{x}_{MC}^2] - \mathrm{E}[\dot{x}_{WR}^2])^2 \mathrm{d}t \tag{14}$$

where

$$\sigma_{\dot{x}}^2 = \frac{1}{T} \int_0^T \mathrm{E}[\dot{x}_{MC}^2] \mathrm{d}t \tag{15}$$

and T is the time period of the harmonic excitation. As nonlinearity increases, the JPDF increases in complexity so the equations fail to solve. The value of nonlinearity at

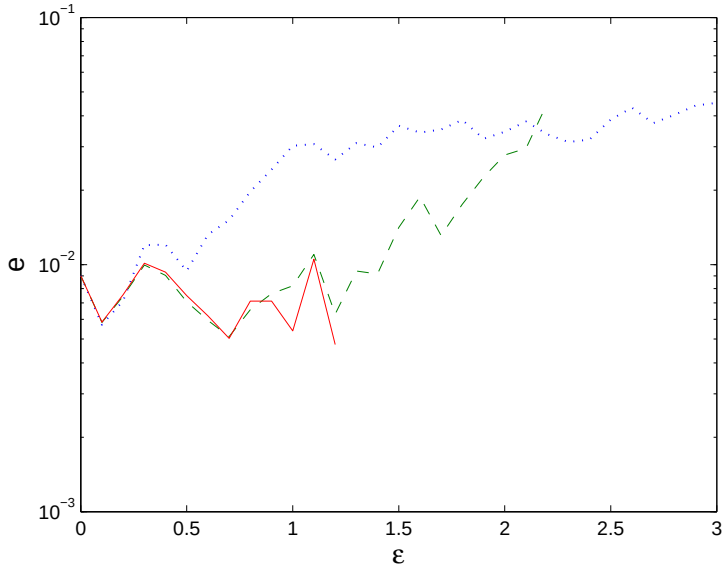

Figure 10: Error, e, against nonlinearity, ϵ for varying truncation values; $N = 3$ (dotted), $N = 4$ (dashed) and $N = 5$ (solid) when $c = 0.5$, $k = 5$, $F = 10$, $\omega = 1$ and $S_0 = 0.5$. Where no error point is plotted, the solution has failed to solve.

which the equations fail to solve is lower the higher the order of truncation of the series due to higher order solutions having worse conditioning. As nonlinearity increases, the higher order solutions are slightly more accurate by this error measure, but may be significantly more accurate if an error measure involving the entire JPDF was used.

Improvements to this method could potentially be made by using a more suitable proposed JPDF and weighting function. A method could be used whereby the weighting functions depend on the JPDF calculated at the previous time-step.[25] Most modifications would likely produce a significantly more computationally intensive solution since orthogonal functions may not exist or would take longer to compute, functions would have to be calculated at each time-step and numerical integration may be necessary for the weighted integrals. Additionally, it is difficult to envisage the form of a proposed JPDF that would give enough flexibility for more complex JPDF shapes.

In summary, this method produces good results if the JPDF varies only slightly from Gaussian. This occurs when nonlinearity is small, damping is large or the noise is small relative to the harmonic excitation such that the JPDF spreads out in an

approximately linear region. More complex JPDF shapes such as the solution in the double response, Figure 3, or chaotic, Figure 4, regions of the Duffing oscillator will most likely require computation using a different method.

4 Conclusions

The combination of harmonic and white noise vibrations is thought to be a useful approximation of realistic excitation. Monte-Carlo simulations were used to illustrate the dynamics of a Duffing oscillator under such excitation, where the response was found to spread out around the deterministic trajectory. For the chaotic case, the noise was found to diffuse the JPDF from a chaotic attractor, although the attractor and therefore the moments were found to settle to a periodic state.

To investigate how a useful solution technique, the global weighted residual method, models these complex responses, two methods from the literature have been extended and applied to this form of excitation. When the JPDF takes the form of a Gram-Charlier type A series, results were seen to become inaccurate and unphysical, even producing negative mean square velocity. However, a Gram-Charlier type C series was found to generate accurate and rapid results when compared to Monte-Carlo and path integration methods.

Despite good solutions within certain parameter ranges, the method has limitations due to the conditioning of the governing equations. When the dynamics of the system requires a JPDF with a geometry far beyond what the Gram-Charlier type C series can produce, the equations become ill-conditioned and fail to solve. The method is therefore useful for responses where the JPDF does not vary significantly from Gaussian such as a weakly nonlinear or highly damped cases.

Funding

The authors would like to thank the EPSRC Doctoral Training Award for funding this research.

References

[1] Hatchell BK, Mauss FJ, Amaya IA et al. Missile captive carry monitoring and helicopter identification using a capacitive microelectromechanical systems accelerometer. *Structural Health Monitoring* 2011; 11(2): 213–224. DOI: 10.1177/1475921711414237.

[2] Megerle B, Rice TS, McBean I et al. Numerical and experimental investigation of the aerodynamic excitation of a model low-pressure steam turbine stage operating under low volume flow. *Journal of Engineering for Gas Turbines and Power* 2013; 135: 012602–012602–7. DOI:10.1115/1.4007334.

[3] Wellens T, Shatokhin V and Buchleitner A. Stochastic resonance. *Reports on Progress in Physics* 2004; 67: 45–105. DOI:10.1088/0034-4885/67/1/R02.

[4] Harne RL, Sun A and Wang KW. An investigation on vibration energy harvesting using nonlinear dynamic principles inspired by trees. *Active and Passive Smart Structures and Integrated Systems* 2015; 9431(94310L): 1–14. DOI: 10.1117/12.2083115.

[5] Roberts JB and Spanos PD. *Random Vibration and Statistical Linearization*. John Wiley and Sons, 1990.

[6] Iyengar RN. A nonlinear system under combined periodic and random excitation. *Journal of Statistical Physics* 1986; 44(5–6): 907–920. DOI:10.1007/BF01011913.

[7] Nayfeh AH and Serhan SJ. Response statistics of non-linear systems to combined deterministic and random excitations. *International Journal of Non-Linear Mechanics* 1990; 25(5): 493–509.

[8] Haiwu R, Guang M, Xiangdong W et al. Response statistic of strongly non-linear oscillator to combined deterministic and random excitation. *International Journal of Non-Linear Mechanics* 2004; 39: 871–878. DOI:10.1016/S0020-7462(03)00070-2.

[9] von Wagner U. On Double Crater-Like Probability Density Functions of a Dufng Oscillator Subjected to Harmonic and Stochastic Forcing. *Nonlinear Dynamics* 2002; 28: 343–355.

[10] Anh ND and Hieu NN. The Duffing oscillator under combined periodic and random excitations. *Probabilistic Engineering Mechanics* 2012; 30: 27–36. DOI: 10.1016/j.probengmech.2012.02.004.

[11] Anh ND, Zakovorotny VL and Hao DN. Responses Probabilistic Characteristics of a Duffing Oscillator under Harmonic and Random Excitations. *VNU Journal of Mathematics - Physics* 2014; 30(1): 39–49.

[12] Cai GQ and Lin YK. Nonlinearly damped systems under simultaneous broadband and harmonic excitations. *Nonlinear Dynamics* 1994; 6: 163–177. DOI: 10.1007/BF00044983.

[13] Haiwu R, Wei X, Guang M et al. Response of a Duffing Oscillator To Combined Deterministic Harmonic and Random Excitation. *Journal of Sound and Vibration* 2001; 242(2): 362–368. DOI:10.1006/jsvi.2000.3329.

[14] Bontempi F and Faravelli L. Lagrangian/Eulerian description of dynamic system. *Journal of Engineering Mechanics* 1998; 124: 901–911.

[15] Kumar P and Narayanan S. Solution of Fokker-Planck equation by finite element and finite difference methods for nonlinear systems. *Sadhana* 2006; 31(4): 445–461.

[16] Langley RS. A finite element method for the statistics of non-linear random vibration. *Journal of Sound and Vibration* 1985; 101(1): 41–54.

[17] Spencer BF and Bergman LA. On the Numerical Solution of the Fokker-Planck Equation for Nonlinear Stochastic Systems. *Nonlinear Dynamics* 1993; 4: 357–372.

[18] Wehner MF and Wolfer WG. Numerical evaluation of path-integral solutions to Fokker-Planck equations. *Physical Review A* 1983; 27(5): 2663–2670.

[19] Yu JS and Lin YK. Numerical path integration of a non-homogeneous Markov process. *International Journal of Non-Linear Mechanics* 2004; 39: 1493–1500. DOI:10.1016/j.ijnonlinmec.2004.02.011.

[20] Xie WX, Xu W and Cai L. Study of the Duffing-Rayleigh oscillator subject to harmonic and stochastic excitations by path integration. *Applied Mathematics and Computation* 2006; 172: 1212–1224. DOI:10.1016/j.amc.2005.03.018.

[21] Narayanan S and Kumar P. Numerical solutions of Fokker-Planck equation of nonlinear systems subjected to random and harmonic excitations. *Probabilistic Engineering Mechanics* 2012; 27: 35–46. DOI:10.1016/j.probengmech.2011.05.006.

[22] Sun JQ and Hsu CS. First-passage time probability of non-linear stochastic systems by generalized cell mapping method. *Journal of Sound and Vibration* 1988; 124(2): 233–248. DOI:10.1016/S0022-460X(88)80185-8.

[23] Er GK. Multi-Gaussian closure method for randomly excited non-linear systems. *International Journal of Non-Linear Mechanics* 1998; 33(2): 201–214.

[24] Er GK. A consistent method for the solution to reduced FPK equation in statistical mechanics. *Physica A: Statistical Mechanics and its Applications* 1999; 262(1–2): 118–128. DOI:10.1016/S0378-4371(98)00362-8.

[25] Di Paola M and Sofi A. Approximate solution of the Fokker-Planck-Kolmogorov equation. *Probabilistic Engineering Mechanics* 2002; 17: 369–384. DOI: 10.1016/S0266-8920(02)00034-6.

[26] Bhandari RG and Sherrer RE. Random Vibrations in Discrete Nonlinear Dynamic Systems. *Journal of Mechanical Engineering Science* 1968; 10(2): 168–174.

[27] Wen YK. Approximate Method for non-linear random vibration. *Journal of the Engineering Mechanics Division* 1975; 101(4): 389–401.

[28] Muscolino G, Ricciardi G and Vasta M. Stationary and non-stationary probability density function for non-linear oscillators. *International Journal of Non-Linear Mechanics* 1997; 32(6): 1051–1064.

[29] Zhang X, Zhang Y, Pandey MD et al. Probability density function for stochastic response of non-linear oscillation system under random excitation. *International Journal of Non-Linear Mechanics* 2010; 45: 800–808. DOI: 10.1016/j.ijnonlinmec.2010.06.002.

[30] Martens W, von Wagner U and Mehrmann V. Calculation of high-dimensional probability density functions of stochastically excited nonlinear mechanical systems. *Nonlinear Dynamics* 2012; 67: 2089–2099. DOI:10.1007/s11071-011-0131-2.

[31] von Wagner U and Wedig WV. On the Calculation of Stationary Solutions of Multi-Dimensional Fokker-Planck Equations by Orthogonal Functions. *Nonlinear Dynamics* 2000; 21: 289–306.

[32] Jin X, Huang Z and Leung YT. Nonstationary probability densities of system response of strongly nonlinear single-degree-of-freedom system subject to modulated white noise excitation. *Applied Mathematics and Mechanics* 2011; 32(11): 1389–1398. DOI:10.1007/s10483-011-1509-7.

[33] Spanos PD, Sofi A and Di Paola M. Nonstationary Response Envelope Probability Densities of Nonlinear Oscillators. *Journal of Applied Mechanics* 2007; 74: 315–324. DOI:10.1115/1.2198253.

[34] Risken H. *The Fokker-Planck Equation: Methods of Solutions and Applications*. 2nd ed. Springer Series in Synergetics. Springer, 1996.

[35] Jung P. Periodically driven stochastic systems. *Physics Reports* 1993; 234(4–5): 175–295. DOI:10.1016/0370-1573(93)90022-6.

[36] Jung P and Hanggi P. Invariant Measure of a Driven Nonlinear Oscillator with External Noise. *Physical Review Letters* 1990; 65(27): 3365–3368.

[37] Naess A. Chaos and nonlinear stochastic dynamics. *Probabilistic Engineering Mechanics* 2000; 15: 37–47. DOI:10.1016/S0266-8920(99)00007-7.

5 Appendix: Path integration method

The path integration method[19] is described in this appendix. For simplicity it is described for a system with a single random variable such as a first order system and can be extended easily to higher dimensions such as the Duffing oscillator. It is based on the principle that the long-term evolution of the PDF can be found by computing the evolution over small time-steps. The PDF at the ith time-step, $p(x^{(i)}, t_i)$, can be

found from the PDF at the previous time-step, $p(x^{(i-1)}, t_{i-1})$, and the transition PDF, $q(x^{(i)}, t_i|x^{(i-1)}, t_{i-1})$ such that

$$p(x^{(i)}, t_i) = \int_{R_s} q(x^{(i)}, t_i|x^{(i-1)}, t_{i-1}) p(x^{(i-1)}, t_{i-1}) \mathrm{d}x^{(i-1)} \tag{16}$$

where R_s is a finite area of state-space that contains all significant probability and the transition PDF $q(x^{(i)}, t_i|x^{(i-1)}, t_{i-1})$ represents the probability of the response being at a position $x^{(i)}$ at one time-step given that it was at position $x^{(i-1)}$ at the previous time-step.

If a good approximation of the transitional PDF can be found, the evolution of the PDF over time can be found from an initial distribution, $p(x^{(0)}, 0)$, with repeated use of equation (16). The equation can be discretised for numerical calculation by splitting state-space into K sub-intervals and each sub-interval into L Gauss-Legendre points such that equation (16) becomes

$$p(x^{(i)}_{mn}, t_i) = \sum_{k=1}^{K} \frac{\delta_k}{2} \sum_{l=1}^{L} c_{kl} q(x^{(i)}_{mn}, t_i|x^{(i-1)}_{kl}, t_{i-1}) p(x^{(i-1)}_{kl}, t_{i-1}) \tag{17}$$

where δ_k is the length of sub-interval k, c_{kl} is the weight of the klth Gauss point at location x_{kl}. The probability of the response being found at the mnth Gauss point at t_i is therefore found by summing the probability given by taking each Gauss point at the previous time-step and multiplying the probability that the response is at this point with the probability that the response travels from this point to the mnth point over a single time-step.

All that remains is to find a suitable transition PDF. For small enough time-steps, a Gaussian approximation is valid such that Gaussian closure can be used to find the mean, $m_1(t)$, and mean square, $m_2(t)$, response from the klth to the mnth Gauss point. The transition PDF becomes

$$q(x^{(i)}_{mn}, t_i|x^{(i-1)}_{kl}, t_{i-1}) = \frac{1}{\sqrt{2\pi}\sigma(t_i)} \exp\left(-\frac{(x_{mn} - m_1(t_i))^2}{2\sigma(t_i)^2}\right) \tag{18}$$

where $\sigma^2(t) = m_2(t) - (m_1(t))^2$. For the case of the Duffing oscillator (equation (1)) under combined harmonic and white noise excitation, the moment equations from

Gaussian closure are

$$\dot{m}_{10} = m_{01} \tag{19}$$

$$\dot{m}_{01} = -cm_{01} - km_{10} - 3\epsilon m_{10}m_{20} + 2\epsilon m_{10}^3 + F\cos(\omega t) \tag{20}$$

$$\dot{m}_{20} = 2m_{11} \tag{21}$$

$$\dot{m}_{11} = m_{02} - cm_{11} - km_{20} - 3\epsilon m_{20}^2 - 2\epsilon m_{10}^4 + m_{10}F\cos(\omega t) \tag{22}$$

$$\dot{m}_{02} = -2cm_{02} - 2km_{11} - 6\epsilon m_{20}m_{11} + 4\epsilon m_{10}^3 m_{01} + \pi S_0 + 2m_{01}F\cos(\omega t) \tag{23}$$

where $m_{ij} = \mathrm{E}[x^i \dot{x}^j]$.

For stationary excitation the transition PDF will be the same at every time-step thus only requires calculation once and can be used repeatedly. For non-stationary excitation the transition PDF will change with time therefore under harmonic excitation, it will change over the period of the excitation. If the period is split into a suitable number of time-steps then that number of transition PDFs can be calculated and used repeatedly for every oscillation of the harmonic excitation. In the simulations above, the time-step is taken as a quarter of the period of the harmonic excitation.